Objective Assessment of the Effects of Tumor Motion in Radiation Therapy

Yijun Ding[*]

College of Optical Sciences, University of Arizona, Tucson, AZ, United States, 85719

Harrison H. Barrett[†]

Department of Medical Imaging and College of Optical Sciences, University of Arizona, Tucson, AZ, United States, 85719

Matthew A. Kupinski[‡]

College of Optical Sciences, University of Arizona, Tucson, AZ, United States, 85719

Yevgeniy Vinogradskiy[§]

Department of Radiation Oncology, University of Colorado School of Medicine, Aurora, CO, United States, 80045

Moyed Miften[¶]

Department of Radiation Oncology, University of Colorado School of Medicine, Aurora, CO, United States, 80045

Bernard L. Jones[**]

Department of Radiation Oncology, University of Colorado School of Medicine, Aurora, CO, United States, 80045

(Dated: May 26, 2019)

Abstract

Purpose: Internal organ motion reduces the accuracy and efficacy of radiation therapy. However, there is a lack of tools to objectively (based on a medical or scientific task) assess the dosimetric consequences of motion, especially on an individual basis. We propose to use therapy operating characteristic (TOC) analysis to quantify the effects of motion on treatment efficacy for individual patients. We demonstrate the application of this tool with pancreatic stereotactic body radiation therapy (SBRT) clinical data and explore the origin of motion sensitivity.

Methods: The technique is described as follows. (1) Use tumor-motion data measured from patients to calculate the motion-convolved dose of the gross tumor volume (GTV) and the organs at risk (OARs). (2) Calculate tumor control probability (TCP) and normal tissue complication probability (NTCP) from the motion-convolved dose volume histograms. (3) Construct TOC curves from TCP and NTCP models. (4) Calculate the area under the TOC curve (AUTOC) and use it as a figure of merit for treatment efficacy. We used tumor motion data measured from patients to calculate the relation between AUTOC and motion magnitude for 25 pancreatic SBRT treatment plans. Furthermore, to explore the driving factor of motion sensitivity of a given plan, we compared the dose distribution of motion-sensitive plans and motion-robust plans and studied the dependence of motion sensitivity to motion directions.

Results: Our technique is able to recognize treatment plans that are sensitive to motion. Under the presence of motion, the treatment efficacy of some plans changes from providing high tumor control and low risks of complications to providing no tumor control and high risks of side effects. Several treatment plans experience falloffs in AUTOC at a smaller magnitude of motion than other plans. In our dataset, a potential indicator of a motion-sensitive treatment plan is that the duodenum is in close proximity to the tumor in the SI direction.

Conclusions: The TOC framework can serve as a tool to quantify the effects of internal organ motion in radiation therapy. With pancreatic SBRT clinical data, we applied this tool to study the change in treatment efficacy induced by motion for individual treatment plans. This framework could potentially be used clinically to understand the effects of motion in an individual patient and to design a patient-specific motion management plan. This framework could also be used in

research to evaluate different components of the treatment process, such as motion-management techniques, treatment-planning algorithms, treatment margins, etc.

Keywords: tumor motion, treatment efficacy, TCP, NTCP, TOC

* Email: dingy@email.arizona.edu; Author to whom correspondence should be addressed. The work was carried out when the author was working at the University of Colorado School of Medicine.
† Email: hhb@email.arizona.edu
‡ Email: kupinski@email.arizona.edu
§ Email: yevgeniy.vinogradskiy@ucdenver.edu
¶ Email: moyed.miften@ucdenver.edu
** Email: bernard.jones@ucdenver.edu

I. INTRODUCTION

In radiation therapy, internal organ motion is a major concern for all tumor sites in the thorax and abdomen, because it decreases the accuracy of radiation delivery [1–5]. Many studies have assessed the effects of tumor motion in terms of dose distribution metrics, such as: mean dose [6], dose-population histograms [7], coverage probability [8] and individual dose-volume histograms [3]. However, none of these studies relate tumor motion to clinical-based endpoints of radiation therapy.

To study the effects of motion on treatment efficacy, we borrowed a generally-accepted concept, 'objective assessment', from the Medical Imaging community. 'Objective' means based on the performance of medically or scientifically relevant tasks [9]. The task in diagnostic imaging is often to detect an abnormality. Many evaluation methods of the performance of this task relate to receiver operating characteristic (ROC) analysis, which depicts the trade-off between the probability of detection (true-positive rate) and the false-alarm fraction (false-positive rate) as the decision threshold is varied. ROC analysis and the area under the ROC curve (AUROC) have been used to assess image quality, compare imaging systems and evaluate reconstruction algorithms [10, 11].

In cancer radiation therapy, the task is to cure or control tumors while reducing the risk of harming normal tissues. The achievement of this task can be measured through two clinically-based endpoints: the tumor control probability (TCP) [12, 13] and the normal tissue complication probability (NTCP) [14, 15], which correspond to the probability of benefits and the risk of side effects, respectively. TCP and NTCP are models relating clinical outcomes to dose received by tumors and organs at risk (OARs). A variety of mathematical models have been presented to describe the dose-response curves obtained from experiments and clinical trials [16], and standardized modules for the calculation of some models are freely available [17–19]. Furthermore, there are major ongoing efforts to incorporate emerging clinical data into TCP and NTCP modeling [20–22].

TCP and NTCP are two inseparable aspects of treatment efficacy, because there are potential trade-offs between the two outcomes. For example, when the treatment dose is increased, TCP increases at the sacrifice of increased NTCP. One way to consider TCP and NTCP simultaneously is to use a therapy operating characteristic (TOC) curve, analogous to an ROC curve. The TOC curve plots TCP vs. NTCP as the treatment dose is varied.

TOC curves reflect the therapeutic ratio between TCP and NTCP.

TOC was first introduced to the radiotherapy community by Mendelsohn and Moore [23, 24] in 1972 for comparison of treatment protocols. Since then, TOC has been applied to optimize the radiation dose in several disease sites [25–28]. More recently, the area under the TOC curve (AUTOC) [29, 30] has been employed as a figure of merit to evaluate segmentation algorithms [31], to assess image quality in radiation therapy [30, 32], to prescribe radiation dose on a per-patient basis [33] and to study treatment efficacy in the field of precision chemotherapy [34]. More specifically, the theory of applying TOC to the study of tumor motion was laid out by Barrett et. al. [30].

Tumor motion blurs the planned dose distribution and leads to a deviation between the intended and delivered dose distributions. When motion causes the OARs to move into the high-dose regions of a treatment plan, NTCP increases. Additionally, when motion causes tumors to move out of the treatment volume, TCP decreases. In this way, motion can decrease TCP and increase NTCP, and hence drag the TOC curve from the upper left corner towards the lower right corner. As a result, AUTOC decreases with tumor motion. Therefore, AUTOC can serve as a figure of merit to study the effect of tumor motion on the efficacy of radiation treatment [30].

To demonstrate the utility of TOC/AUTOC in studying the clinical effects of motion in radiotherapy, we applied the TOC framework in pancreatic Stereotactic Body Radiation Therapy (SBRT). In recent years, multiple clinical trials have shown encouraging clinical outcomes of pancreatic cancer patients after SBRT [35–38]. However, the safe delivery of pancreatic SBRT is hindered by tumor motion. First, since the motion of the pancreas is often highly irregular, it is hard to account for by the four-dimensional computed tomography (4DCT) images acquired at the time of simulation [39–41]. Secondly, the pancreas is located in close proximity to the duodenum, which is highly sensitive to radiation and hence limits dose escalation in pancreatic SBRT [42].

The purpose of our paper is twofold: first, to develop TOC as a tool and AUTOC as a figure of merit for objective (task-based) assessment of the effects of tumor motion on treatment efficacy, and second, to demonstrate the utility of this approach using real-world examples with clinical data. We accomplished this purpose in three steps. First, we developed a TOC framework for quantifying the effect of motion on clinical endpoints. Next, we utilized daily motion data measured from patients in conjunction with clinical treatment

plans for pancreatic cancer. With these data, we applied the TOC framework to investigate the robustness of individual patient plans to internal organ motion during treatment and explore the origin of motion sensitivity. Our goal of this paper is to develop TOC and AUTOC as tools in Medical Physics research to relate the details of patient treatment to clinical endpoints.

Three supplemental materials are attached: Supplement A provides the TOC analysis of a different TCP model; Supplement B provides the TCP model, AUTOC data for all patients, an uncertainty analysis of AUTOC on model parameters, a comparison of clinical dose-escalated plans and original plans, and an outlier tumor trajectory; and Supplement C provides a list of acronyms.

II. MATERIALS AND METHODS

In this section, we first present the TOC framework in the study of tumor motion; then we introduce the TCP and NTCP models; and lastly, we discuss the details of an example application with clinical data.

A. A TOC framework for studying the effects of tumor motion on treatment efficacy

To evaluate effects of tumor motion, one needs to calculate the motion-blurred dose distributions. Since we are not concerned with the effects of image noise, segmentation uncertainty, or errors in dose calculation, we can assume the structure boundaries are exact and the dose calculation is accurate. Radiation delivered to a structure in the presence of tumor motion is the dose accumulated within the structure boundary over time:

$$D(\mathbf{R}) = \int_0^T \mathrm{dt}\ f(\boldsymbol{\mathcal{T}}_t \mathbf{R}, t), \tag{1}$$

where D is the accumulated dose distribution, $\mathbf{R}$ is a point in the 3D space, T is the delivery time of a treatment fraction, f is the dose rate and $\boldsymbol{\mathcal{T}}_t$ is a transformation operator describing the motion and deformation of the structure at time t. Note that when $\boldsymbol{\mathcal{T}}_t$ is a unit operator (corresponding to no motion), $D(\mathbf{R})$ is the planned dose distribution, or static dose distribution $D_s(\mathbf{R})$.

The main effect of organ motion in intensity-modulated radiotherapy is an averaging of the static dose distribution over the path of the motion [43]. If the static dose distribution is not affected much by the internal organ motion, the motion-blurred dose can be calculated by:

$$D(\mathbf{R}) = \frac{1}{T}\int_0^T \mathrm{dt}\ D_s(\mathbf{R} - \Delta\mathbf{R}(t)), \tag{2}$$

where $\Delta\mathbf{R}(t)$ is the three-dimensional displacement of the organ at time t. We refer to this $D(\mathbf{R})$ as the motion-convolved dose. If the tissue of interest is mostly soft tissue and the organ deformation is not severe, Equation (2) is a good approximation. Otherwise, for example, if lung tissues and bones exist in the volume of interest, Equation (1) should be used in the calculation.

The TOC curve is a parametric plot of TCP versus NTCP with the overall dose as a continuous hidden parameter. The overall dose can be varied by changing the beam current or the exposure time. To calculate TCP and NTCP at different overall dose levels, we assume that the clinical dose distribution scales by the same factor at each position $\mathbf{R}$,

$$D(\mathbf{R}) = rD_0(\mathbf{R}), \tag{3}$$

where $D_0(\mathbf{R})$ is the dose distribution at some reference overall dose and r is the ratio of the overall dose to the reference dose. As the overall dose increases, TCP and NTCP both increase and form an ascending TOC curve, as shown in Figure 1.

A TOC curve has two nice properties: (1) it can be generated for each dose distribution $D_0(\mathbf{R})$; and (2) it provides information about treatment efficacy for all possible doses. For illustration, three target dose levels, 30, 50 and 70 Gy, are marked on the TOC curves in Figure 1.

In current clinical practice, if the treatment dose is escalated, new treatment plans would be generated to satisfy a different set of dose constraints. We refer to this new plan as a clinical dose-escalated plan. This new treatment plan will produce a new TOC curve. However, a TOC curve generated by scaling dose of the original plan, as described by Equation (3), is a good approximation of the family of TOC curves generated from clinical dose-escalated plans, at least for the purpose of studying the effects of motion. To demonstrate this, we compare dose scaling and clinical dose escalation in terms of the TOC analysis in the Results section and Supplement B.

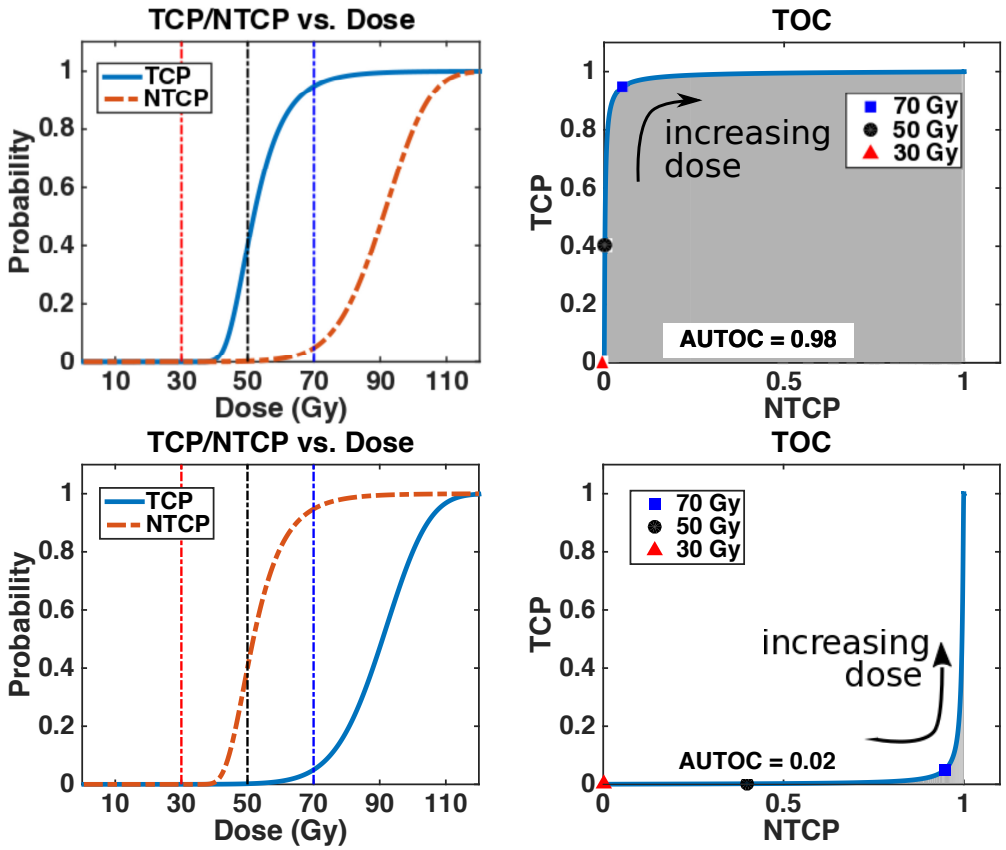

FIG. 1. TCP, NTCP and TOC curve of a good treatment plan (top) and a bad treatment plan (bottom). AUTOC is the area indicated in grey.

The therapeutic efficacy of a radiotherapy treatment plan can be evaluated by the AUTOC. An ideal treatment plan, which treats the patient without risk of any injuries, has an AUTOC of 1, as shown in Figure 1 top row. Conversely, an absolutely bad plan, which damages normal tissue while offering little chance of tumor control, occupies the lower right corner of the plot and thus has an AUTOC close to 0, as shown in Figure 1 bottom row.

Each motion-blurred dose distribution will produce a TOC curve; hence an AUTOC value can be calculated for each combination of a treatment plan and a motion trajectory.

B. TCP and NTCP models

TCP is a product of the probabilities to control each voxel in the gross tumor volume (GTV)[16]:

$$TCP = \prod_{i=1}^{M} P(D_i)^{V_i/V_{ref}}, \tag{4}$$

where M is the number of voxels, D_i is the dose to the i^{th} voxel, $P(D_i)$ is the local control probability of the i^{th} voxel, V_i is the volume of the i^{th} voxel, and V_{ref} is the reference volume of the TCP model [44]. The voxel control probability, $P(D_i)$, can be modeled mechanistically or empirically. A mechanistic TCP model assumes the following: (1) a tumor consists many tumor clonogens; (2) curing a tumor requires eradication of all tumor clonogens; and (3) a mechanistic model can be used to describe the probability of cell death [45]. In contrast, empirical models take the form of a two-parameter sigmoid-shaped mathematical function [13].

We briefly summarize a mechanistic model here and introduce an empirical model in Supplement A. The mechanistic model assumes that the number of tumor clonogens follows a Poisson distribution with mean NS, where N is the number of clonogens in the tumor before treatment and S is the fraction of cells that survive radiation treatment. Tumor control occurs when all tumor clonogens have been eradicated:

$$P(D) = e^{-NS(D)}, \tag{5}$$

where D is the dose. The fraction of surviving cells follows

$$S(D) = \int_0^\infty d\alpha \; p(\alpha) S(D|\alpha) \tag{6}$$

where α describes the radiation sensitivity of cells, $p(\alpha)$ is a probability density function of the radiation sensitivity and $S(D|\alpha)$ is the surviving rate of cells given the radiation sensitivity α. Since cell death is a mechanistic consequence of repair/misrepair of radiation-induced double-strand DNA breaks, $S(D|\alpha)$ often takes the Linear-Quadratic (LQ) form [46]:

$$S(D|\alpha) = \exp[-\alpha D(1 + \frac{D/n}{\alpha/\beta})], \tag{7}$$

where $\alpha/\beta = 10$ Gy is generally accepted for tumors and n is the total number of treatment fractions. The tumor heterogeneity model $p(\alpha)$ can be derived from clinical data or experimental data.

A commonly used NTCP model is a Lyman-Kutcher-Burman (LKB) model [14, 15], which employs an empirical form and attempts to incorporate structural knowledge of the OAR. The model is defined as following:

$$NTCP(t) = \frac{1}{\sqrt{2\pi}} \int_{-\infty}^{t} \mathrm{dx}\ \exp(-\frac{x^2}{2}). \tag{8}$$

The upper limit of the integration t is defined as

$$t = \frac{\mathrm{EUD} - TD_{50}}{m \times TD_{50}}, \tag{9}$$

where m is a model parameter that relates to the inverse slope of the NTCP curve, TD_{50} is the dose that corresponds to a 50% probability of complications, and EUD is the equivalent uniform dose defined as

$$\mathrm{EUD} = \left(\sum_i D_i^{1/l} \frac{V_i}{V_{tot}} \right)^l, \tag{10}$$

where D_i is the dose in the i^{th} voxel, V_i is the volume of the i^{th} voxel, V_{tot} is the total volume of the organ, and l is a model parameter related with the structure of the OAR. The model considers the OAR as many functional subunits (FSUs) organized in series ($l \ll 1$), in parallel ($l = 1$) or a mixture of both ($0 < l < 1$) [47]. For an organ structured in series, elimination of any FSUs results in side effects; on the contrary, a parallel organ can tolerate a larger irradiated volume.

If an NTCP model is derived based on a different fractionation schedule, the biological effective dose (BED) [48] can be used to convert the dose. A commonly used form of BED is given by

$$\mathrm{BED} = D(1 + \frac{D/n}{\alpha/\beta}), \tag{11}$$

where D is the dose over n fractions. However, the dose conversion should be used with caution, especially when comparing hypofractionated regimens with conventional fractionation [49].

C. Application of TOC framework in pancreatic SBRT

We retrospectively analyzed clinical treatment plans of 25 patients diagnosed with pancreatic adenocarcinoma and treated with volumetric-modulated arc therapy (VMAT) at our institution. Treatment plans were designed to deliver 33 Gy in five fractions. The Eclipse^{TM}

treatment planning system (Varian Medical Systems, Palo Alto, CA) was used for planning and dose calculation. Treatment plans from these clinical cases were analyzed under an institutional review board (IRB) approved retrospective research protocol.

Tumor motion data were collected in a previous study of SBRT for pancreatic cancer [5]. Time-resolved tumor positions were estimated from raw cone-beam computed tomography (CBCT) projection images with an automated template-matching algorithm [50–52]. Fiducial markers were implanted close to a tumor, and the positions of the fiducial markers were used as surrogates for the tumor location. A total of 91 trajectories of pancreatic tumors were collected from 19 patients. The patients were wearing compression belts at the time of data collection. Each trajectory contained 3D position data over 1 minute at a sampling rate of 15 Hz. The three directions of the trajectories are referred to as superior-inferior (SI), left-right (LR), and anterior-posterior (AP), respectively. For each trajectory, the magnitude of motion is defined as the 95% confidence interval (CI) of motion range in the SI direction.

For the TCP model, we used the mechanistic model described previously and assumed a model of tumor heterogeneity, $p(\alpha)$, derived from lung SBRT data [53]. The form and parameters of $p(\alpha)$ are provided in Supplement B. For the NTCP model, we used a LKB model derived for pancreatic SBRT by Murphy et. al. [49]. The model predicts Grade II—IV duodenal toxicity [54], including duodenum ulcer, gastrointestinal hemorrhage, duodenum stricture and duodenum perforation for a treatment regimen of 25 Gy in a single fraction. The model parameters are: $TD_{50} = 24.6$ Gy, $m = 0.23$, and $l = 0.12$ [49]. To use this NTCP model, we used BED to convert the dose distribution per five fractions to the equivalent dose obtained using a single-fractionation regimen.

We defined the overall dose as the dose prescribed to at least 95% of the planning target volume (PTV). We simulated treatment plans with overall dose ranging 0—120 Gy by scaling the 33-Gy-treatment plans according to Equation (3). To calculate AUTOC, we extrapolated the TOC curve to a point where NTCP equals to 1 and TCP equals to the TCP value at 120 Gy.

We assumed rigid motion of the volume containing the pancreas and the duodenum. The radiation delivered under the presence of a tumor trajectory is calculated according to Equation (2), which averaged the static dose distribution over the tumor trajectory. The accumulated dose under the presence of motion was used to calculate the DVH for the GTV

and the duodenum.

Firstly, we chose five tumor trajectories to show how TCP, NTCP and TOC curves change with the magnitude of motion. The five tumor trajectories included one ideal trajectory with no motion and four motion trajectories. The four motion trajectories corresponded to the 25^{th}, 50^{th}, 75^{th} and 99^{th} percentile of all 91 tumor trajectories in terms of the magnitude of motion, respectively.

Secondly, all 91 tumor trajectories were used to study the relation between AUTOC and the magnitude of motion. For each treatment plan and a tumor trajectory combination, a TOC curve and an AUTOC value were calculated. For each treatment plan, 91 AUTOC values were plotted against the motion magnitude.

Thirdly, to approximate the average trend of AUTOC vs. motion, we used a mathematical motion model to simulate a set of tumor motion trajectories. The motion model, which is based on lung tumor data [55, 56], assumes the position of the tumor $\boldsymbol{s}$ as a function of time t:

$$\boldsymbol{s}(t) = \boldsymbol{s}_0 - \boldsymbol{S}\cos^{2n}\left(\frac{\pi t}{\tau} - \boldsymbol{\phi}\right), \tag{12}$$

where $\boldsymbol{s}_0$ is the position of the tumor at exhalation, $\boldsymbol{S}$ relates to the magnitude of motion, τ is the period of the respiratory cycle, $\boldsymbol{\phi}$ is the starting phase, and n describes the asymmetry of the motion trajectory. Different trajectories may assume different asymmetry parameter n. Higher values of n means more dwell time in the exhale position. The starting phase $\boldsymbol{\phi}$ may be different in different directions and this is referred to as hysteresis. We assumed the following parameters: $S_{LR}/S_{SI} = 0.48$, $S_{AP}/S_{SI} = 0.54$ (patient motion data), $\tau = 3.6$ seconds, $\phi_{LR} - \phi_{SI} = 0.5$ seconds, $\phi_{AP} - \phi_{SI} = 0.1$ seconds [55] and $n = 3$. To reemphasize, we did not attempt to fit patient motion data into the mathematical model. The motion model was used to approximate the average trend of AUTOC vs. motion.

In addition, to examine the effects of uncertainties in the parameters of TCP/NTCP models, we calculated AUTOC for varying model parameters.

Furthermore, it is of interest to compare a clinical dose-escalation with dose scaling from the original plan. We replanned three motion-sensitive patients and three motion-robust patients at 50 Gy per five fractions. The 50 Gy was chosen due to the practical reason that many of the dose constraints are clinically unknown for doses much higher than current practices. We compared the new plans and the original plans in terms of TOC curves and AUTOC values.

Last but not least, we explored contributing factors to a plan's motion sensitivity. We selected six plans, which consisted of the three most sensitive and the three least sensitive to motion, and compared their dose distributions and tumor volumes. In addition, we compared AUTOC of three-dimensional (3D) motion and one-dimensional (1D) motion, where the 3D motion data were measured from patient and the 1D motion assumed same SI motion as the 3D motion but no motion in the AP direction and the LR direction.

III. RESULTS

A. Motion sensitivity of treatment plans

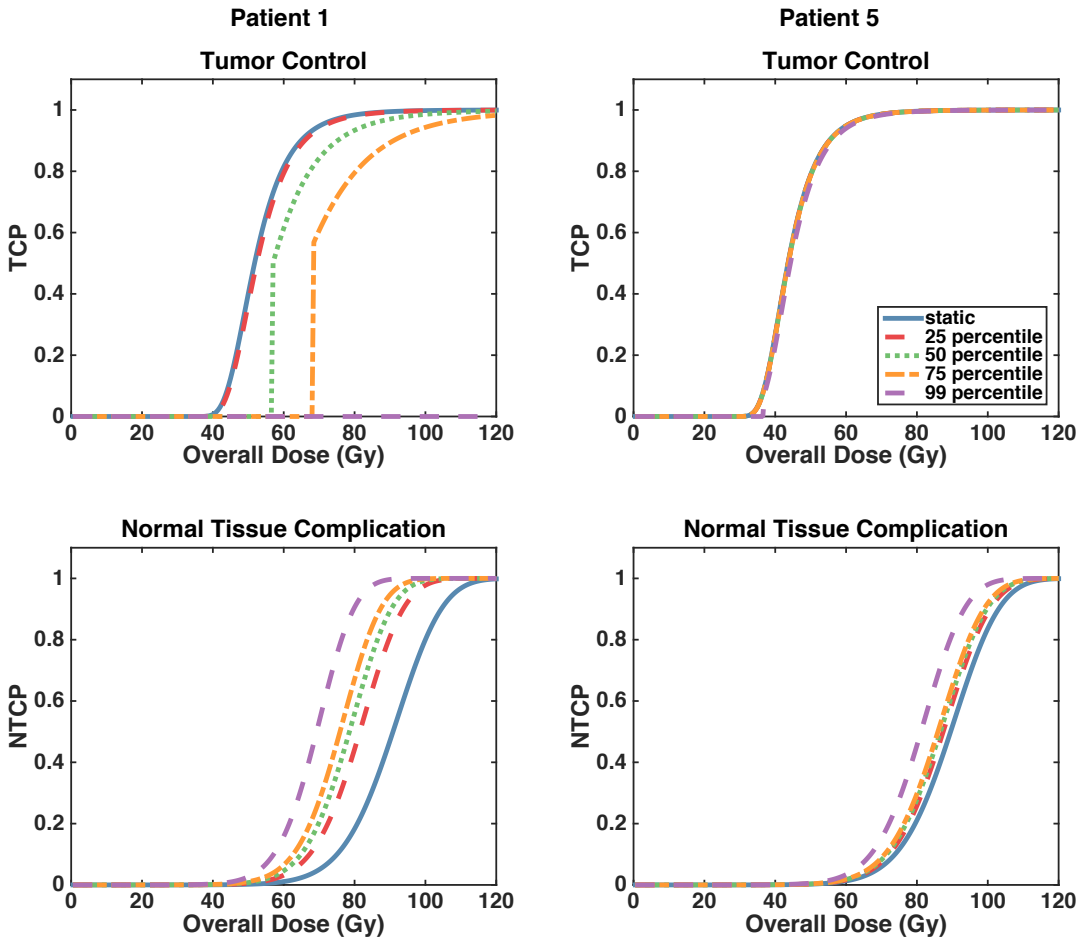

FIG. 2. The effects of motion on TCP and NTCP for Patient 1 (left) and Patient 5 (right). Top row: TCP vs. Overall dose. Bottom row: NTCP vs. Overall dose. Different line colors and styles show four motion trajectories and the ideal scenario of no tumor motion. The four motion trajectories correspond to the 25^{th}, 50^{th}, 75^{th} and 99^{th} percentile of all tumor trajectories in terms of motion magnitude.

We plot TCP/NTCP as functions of the overall dose in Figure 2 for two treatment plans. The 91 tumor trajectories produce 91 TCP plots and 91 NTCP plots for each treatment plan. In this figure, results of five tumor trajectories, which have been specified in the Methods section, are presented. The shape of the TCP and NTCP plots change with the magnitude

of motion. As the magnitude of motion increases, the shape of the TCP vs. overall dose plots (top row) changes dramatically for Patient 1 (left column) and barely changes for Patient 5 (right column); the change in NTCP plots (bottom row) of Patient 1 is slightly larger than that of Patient 5.

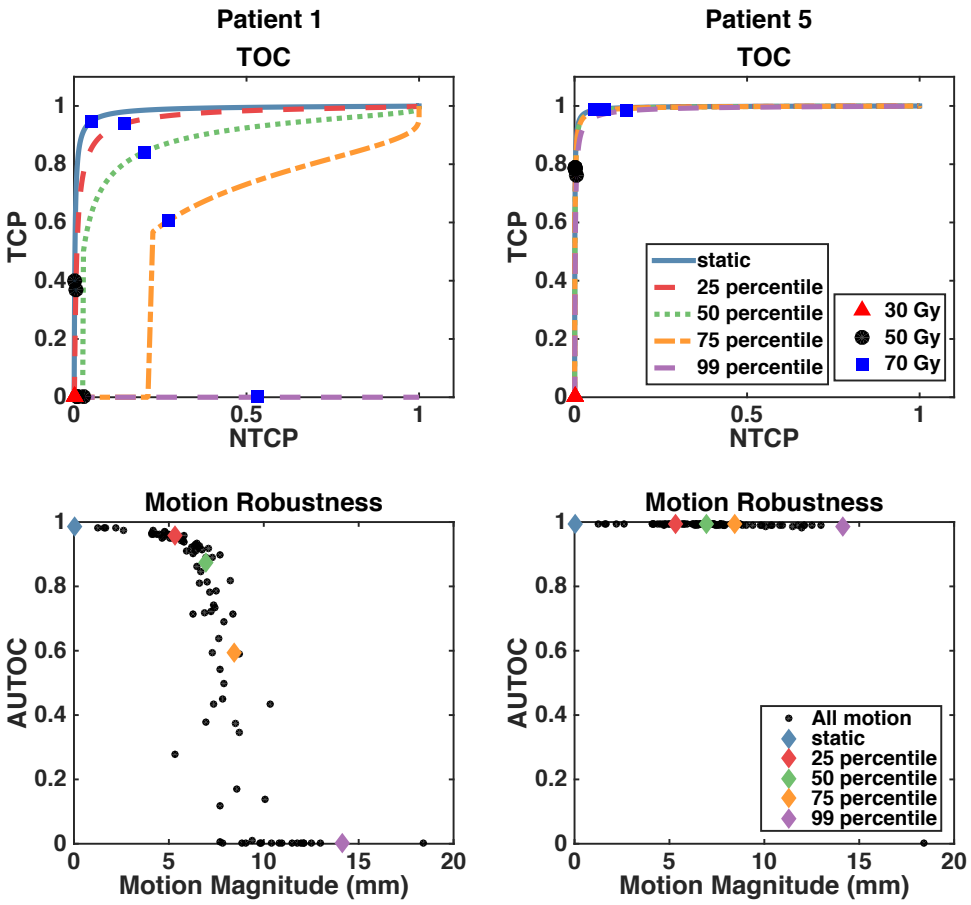

FIG. 3. The effects of motion on TOC curves and AUTOC values for Patient 1 and Patient 5. In the top row, TOC curves of the same five selected trajectories as in Figure 2 are plotted in different line colors and styles. In the bottom row, AUTOC are plotted as a function of motion magnitude. Each black dot is from one tumor trajectory; the diamonds highlights the five selected trajectories. For reference, three target dose levels, 30 Gy, 50 Gy and 70 Gy/5 fractions are indicated on the TOC curves in triangle, circle and square, respectively.

To view TCP and NTCP jointly, we combine TCP and NTCP into TOC curves and

display the results in the upper row of Figure 3, where the same five tumor trajectories as in Figure 2 are presented. As the magnitude of motion increases, the TOC curves of Patient 1 (left column) shift from the upper left corner (blue, beneficial to the patient) to the lower right corner (purple, harmful to the patient), while the TOC curves of Patient 5 (right column) consistently occupy the upper left corner (beneficial to the patient).

Each TOC curve provides one AUTOC value. When all 91 tumor trajectories are considered, there are 91 AUTOC values. These AUTOC values are shown by the scatter plot in the lower row of Figure 3, and the five chosen tumor trajectories are indicated in diamonds. The motion magnitude is the 95% CI range in the SI direction. The AUTOC of Patient 1 decreases with increasing motion magnitude, while the AUTOC of Patient 5 stays close to 1. In other words, the treatment plan of Patient 1 is sensitive to motion, while the treatment plan of Patient 5 is robust to motion.

For reference, we list conventional motion-sensitivity metrics for the two patients. Since there is a lack of consensus on conventional metrics, three metrics are chosen to our best knowledge: the dose covering 98% of the GTV (D_{98}), the maximum dose covering at least 0.1 cm^3 of the duodenum ($D_{0.1cc}$) and the volume of the duodenum that receives more than 33 Gy (V_{33}). When no motion is considered, the dose volume metrics for the two patients are: $D_{98} = 33.7$ Gy, $V_{33} = 0$ cm^3, $D_{0.1cc} = 25.4$ Gy for Patient 1; $D_{98} = 34.2$ Gy, $V_{33} = 0$ cm^3, and $D_{0.1cc} = 27.3$ Gy for Patient 5. Across all tumor trajectories, D_{98} is 30 ± 6 Gy (mean $\pm$ standard deviation) for Patient 1 and 33 ± 2 Gy for Patient 5; $D_{0.1cc}$ is 32 ± 3 Gy for Patient 1 and 29 ± 1 Gy for Patient 5; V_{33} is 0.12 ± 0.12 cm^3 for Patient 1 and 0.00 ± 0.01 cm^3 for Patient 5. Those values show that the treatment plan of Patient 1 is more sensitive to motion. However, it is hard to combine those physically-based values into one figure of merit that is related to treatment efficacy.

As a side reference, three target dose levels, 30 Gy, 50 Gy and 70 Gy per 5 fractions to the PTV, are indicated on the TOC curves in triangle, circle and square, respectively.

AUTOC of simulated tumor trajectories can be used to approximate the mean trend of AUTOC calculated from real patient motion, as shown in Figure 4. The results of all 25 patients are presented in Supplement B.

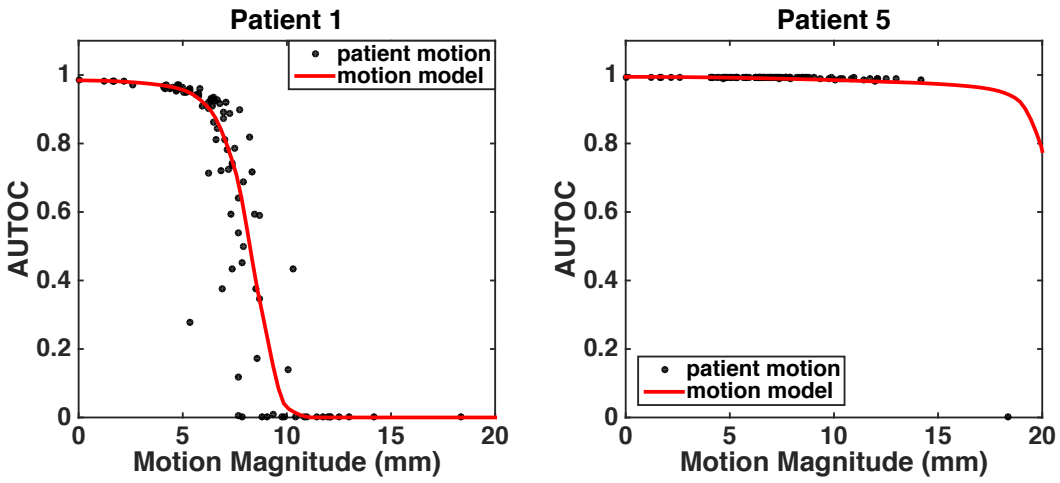

FIG. 4. AUTOC vs. motion magnitude for tumor motion measured from patient (black dots) and a set of simulated tumor trajectories (red line). The simulated tumor trajectories are employed to approximate the mean change of AUTOC with motion for real motion trajectories.

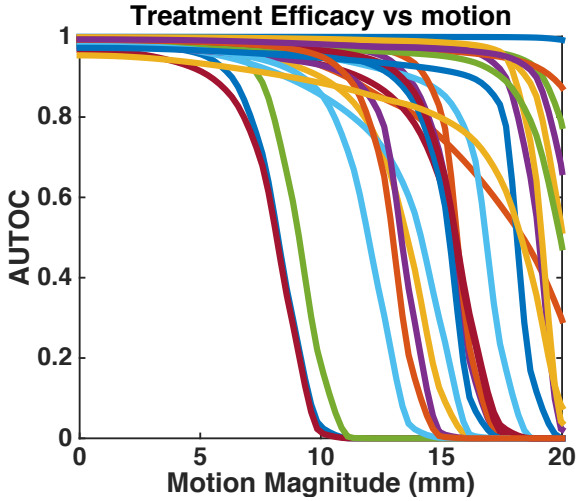

FIG. 5. AUTOC vs. motion magnitude for all 25 patients. The motion magnitude is defined as the 95% CI range in the SI direction. Each line is the AUTOC of one treatment plan, where the AUTOC is calculated based on tumor trajectories generated from the motion model.

One can discern the motion sensitivity of different treatment plans by the relationship between AUTOC and motion magnitude. Figure 5 presents the AUTOC (calculated from the motion model) as functions of motion magnitude for all 25 treatment plans, where each line represents one treatment plan. Some plans suffer a sudden decrease in treatment efficacy

at a motion magnitude of around 6 mm (95% CI of SI motion). Other plans are robust to tumor motion. In this way, AUTOC can quantify the motion sensitivity of a given plan.

The uncertainties in AUTOC induced by the uncertainties in parameters in the TCP/NTCP model, including $\bar{\alpha}$, m, l and TD_{50}, are presented in Supplement B. More specifically, $\bar{\alpha}$ is the average radiation sensitivity of the cells in the TCP model; m relates to the inverse slope of the NTCP curve; l describes the organization structure of the FSUs in the OARs; and TD_{50} is the dose that corresponds to 50% of complications. When the model parameters are within the range of uncertainties reported [49, 53], the varying parameters affect the AUTOC values, but do not drastically influence the shape of the AUTOC–vs.–motion plots.

B. Dose scaling vs. clinical dose escalation

Clinical dose-escalated plans (replanned) of three motion-robust patients and three motion-sensitive patients are compared to their original plans (the 33 Gy plan) in terms of AUTOC. We present the results of one patient in this section and the results of the other five patients in Supplement B. If the original plan is robust to motion, the differences between the clinical dose-escalated plan and the original plan are almost negligible in terms of TOC and AUTOC, as shown in Supplement B. To show a nontrivial case, we present results of one motion-sensitive patient in Figure 6. The left panel shows TOC curves of five selected motion trajectories (same as in Figure 2). The right panel shows AUTOC values of all motion trajectories.

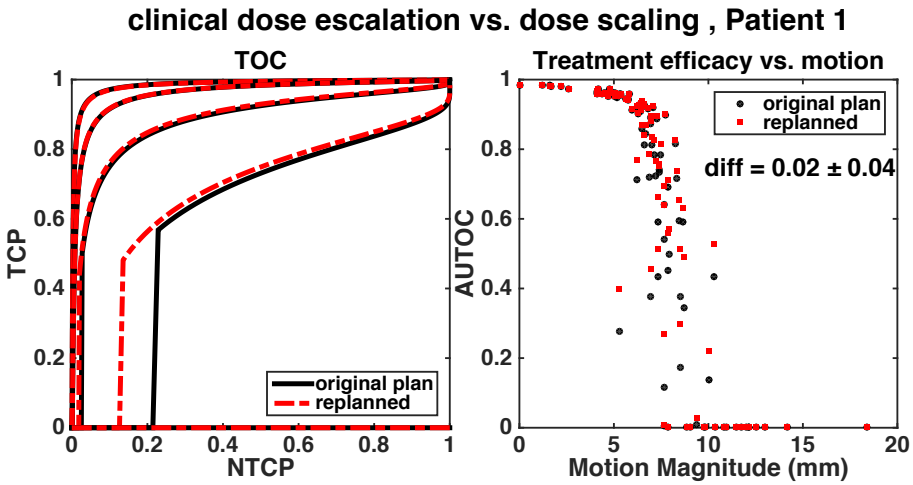

FIG. 6. Comparison of a clinical dose-escalated plan to an original plan in terms of TOC curves and AUTOC values. The clinical dose-escalated plan is replanned to 50 Gy per 5 fractions. The original plan is 33 Gy per 5 fractions.

The difference between the two sets of AUTOC values is 0.02 ± 0.04 (mean $\pm$ standard deviation), which is not significantly different from 0. In fact, none of the six cases have shown significant difference between the new plan and the original plan in terms of AUTOC. Therefore, despite the current clinical practice of altering treatment plans when the dose is escalated, TOC curve with dose scaling is a good surrogate for treatment efficacy over all doses, at least for the purpose of evaluating the effects of motion.

C. Motion-sensitive vs. motion-robust plans

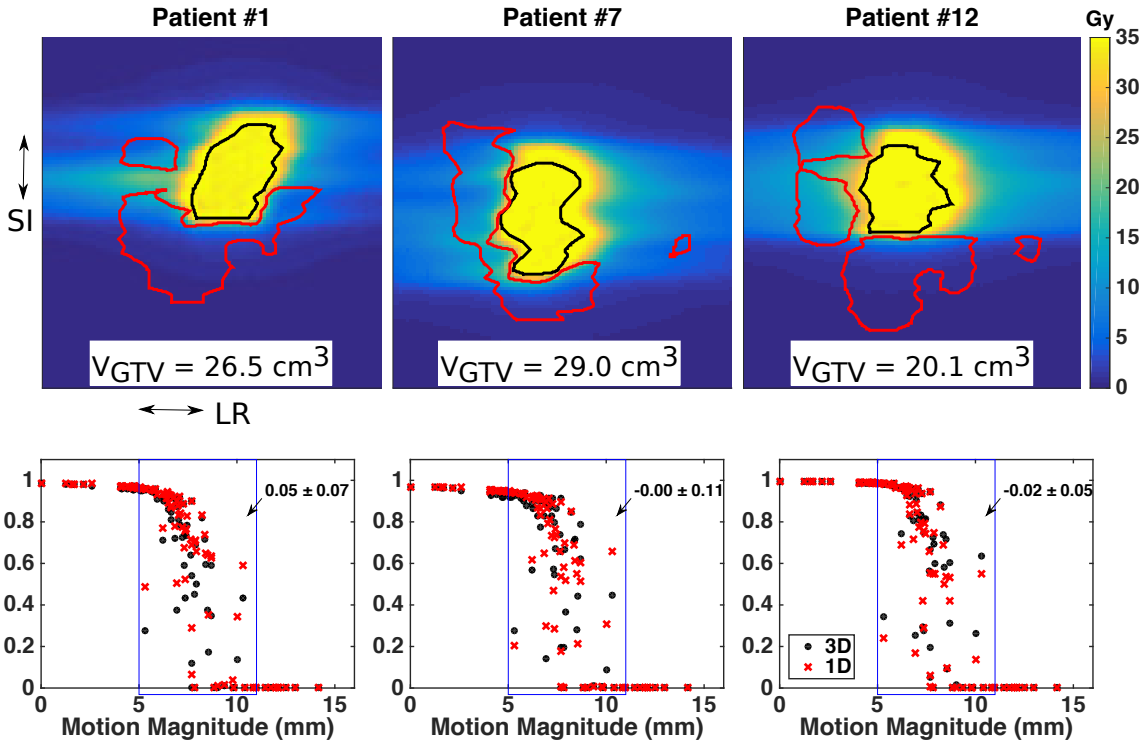

FIG. 7. Dose distribution and AUTOC plots for the three treatment plans that are most sensitive to motion. Each column corresponds to one patient. Top row: one coronal plane slice of the 3D dose distribution in Gy. The slices are chosen to show close proximity between the tumors (black outlines) and the duodenums (red outlines). The size of the slices is 15×15 cm^2. Bottom row: AUTOC vs. motion magnitude for 3D motion (black dots) and 1D SI motion (red crosses). For each plan, the annotation shows the mean and standard deviation of the difference between AUTOC of the 1D motion and 3D motion with magnitude between 5 mm and 11 mm (blue box).

The dose distributions of three motion-sensitive plans and three motion-robust plans are shown in the upper rows of Figure 7 and Figure 8, respectively. For each plan, a 2D coronal-plane slice of the 3D dose distribution is presented. The slice is chosen at an AP location where the tumor boundary (black line) is closest to the duodenum boundary (red line). The orientation of the dose-distribution plots is as follows: the SI direction is along the y axis, and the LR direction is along the x axis. The motion sensitivity of the plans is shown by the AUTOC plots in the lower rows of the two figures. In a motion-sensitive plan, the duodenum

tends to wrap around the tumor tightly in the SI direction (Patient 1, 7 and 12). When the tumor is approaching the duodenum from the LR direction (Patient 24), the treatment plan is robust to tumor motion.

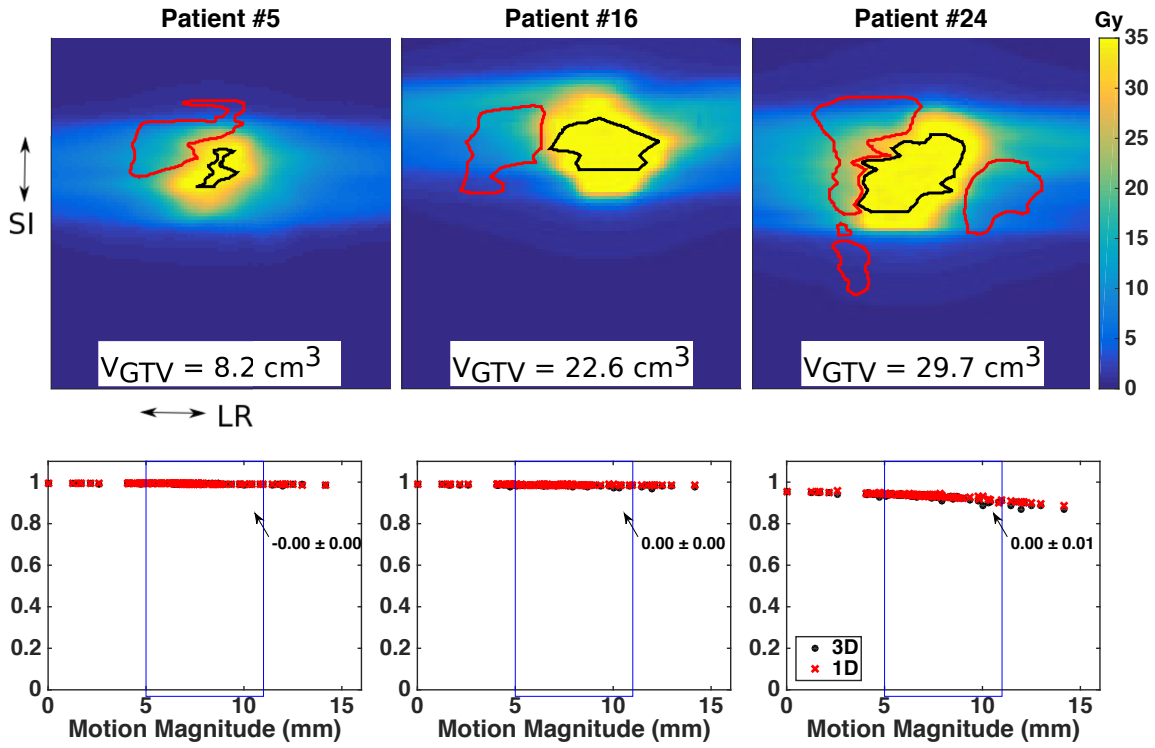

FIG. 8. Dose distribution and AUTOC plots for the three treatment plans that are least sensitive to motion. Details see caption of Figure 7.

In the AUTOC plots, results calculated from 3D tumor-motion trajectories measured from patients are plotted in black dots. AUTOC values calculated from 1D tumor trajectories are plotted in red crosses. For the motion-robust plans (Figure 8), the AUTOC values of the 1D motion are very close to that of the 3D motion. For the motion-sensitive plans (Figure 7), the 1D and 3D results do not match exactly, but they follow the same trend. The range of motion magnitude where 1D and 3D results are significantly different is 5—11 mm, as indicated by the blue boxes in the plots. For tumor trajectories with motion magnitude in this range, the differences between the 1D and 3D AUTOC values are 0.05 ± 0.07, -0.00 ± 0.11 and -0.02 ± 0.05 for the three motion-sensitive plans and are almost 0 for the three motion-robust plans. This indicates that the SI motion is the main contributing factor to the motion-induced changes in AUTOC for the six patients we studied.

The tumor volume of the six patients are displayed on the dose maps in Figure 7 and Figure 8. If we define the motion sensitivity of the three motion-sensitive plans as 1 and the three motion-robust plans as 0, the correlation coefficient between the motion sensitivity and the tumor volume is 0.34 with p-value equals to 50%. Based on these six patients, there is no significant correlation between tumor volume and motion sensitivity.

In summary, a potential indicator of a motion-sensitive plan is that the tumor is in close proximity to the duodenum in the SI direction. The anisotropic behavior of motion-robustness in direction, or the predilection of the 'SI direction', can be explained by a combination of the following two facts: first, the gradient of radiation field at the tumor-duodenum boundary is larger in the SI direction compared to that in the AP and LR directions as shown in Figure 7 and Figure 8; and second, the magnitude of motion in the SI direction is larger than that in the AP and LR directions [5].

IV. DISCUSSION

In research studies and clinical trials, the most important endpoints involve the outcomes of the patients being treated. In treatment of cancer, achieving tumor control while minimizing side effects is the primary goal. Studies that can relate treatment parameters to these outcomes have a greater chance of obtaining clinically significant results. However, in the field of medical physics research, it can be extremely challenging to relate more esoteric characteristics of treatment (e.g. tumor localization accuracy, radiotherapy plan quality, motion management strategies, etc.) to clinical outcomes. The value of AUTOC as a tool for medical physics research is that it can use prior clinical results to distill complex, multi-dimensional data (such as changes in the 3D dose distribution) to a single figure of merit for evaluation. In this way, the true clinical significance of a given research question can be answered.

Our results demonstrate the power of AUTOC in quantifing the clinical effects of motion on aggressive treatments such as pancreatic SBRT. It is important to understand the potential risks caused by tumor motion during radiotherapy, as motion affects all tumor sites in the thorax and abdomen. TOC provides an intuitive way to simultaneously quantify the effects of motion on TCP and NTCP. Furthermore, AUTOC provides a quantitative measure of the changes in treatment efficacy under different motion conditions. By relating

motion magnitude to AUTOC, we were able to recognize plans that were sensitive to tumor motion. Additionally, we were able to use AUTOC to explore which components of motion were driving these treatment deficiencies, and what aspect of patient anatomy was the main contributor to the motion sensitivity of a given plan.

Based on these results, one can imagine clinical scenarios in which the TOC framework is used to tailor an individualized treatment plan for a given patient's motion profile. In the simplest case, one could derive the maximum amount of motion allowable for a given treatment plan, and use that information to select an appropriate motion management strategy for that patient. This requires further work, because the AUTOC value does not decrease monotonically with motion due to variations in patient motion data, as shown for Patient 1 in Figure 4 (black dots). A naive way to calculate allowable motion is to set an arbitrary threshold on AUTOC and calculate the maximum magnitude of motion that ensures AUTOC being larger than the threshold. The threshold can be chosen based either on all tumor trajectories (black dots in Figure 4) or the mean trend (red line in Figure 4). A more sophisticated method to select the optimized threshold involves: (1) an ROC curve that plots the true positive rate against the false positive rate at various AUTOC threshold settings and (2) calculating optimal threshold value based on the cost of misclassification of a tumor trajectory on whether it is safe for the treatment or not. How to optimally select a threshold on AUTOC is an interesting topic for future work.

Another approach could be to identify plans that need replanning using robust optimization, which incorporates motion information into the IMRT optimization process [57]. Building on this, it may be possible to include TOC framework in the plan optimization process, and build a treatment plan that is robust to motion. For example, measures, such as AUTOC values at a given motion magnitude or the areas under the AUTOC-motion curve, may serve as guides to optimize treatment plans. Going even further, one could perform a detailed motion evaluation at the time of simulation, and use this information to design an individualized treatment fractionation which achieves TCP values as high as possible. To achieve these goals, further work is needed to understand exactly which factors cause a plan to be sensitive or robust to motion.

Other applications of the TOC analysis include: evaluating segmentation algorithms, comparing motion-management techniques, assessing the effects of using molecular imaging in therapy planning, evaluating and optimizing internal radiotherapy with the sodium iodide

symporter [30]. A computational framework which employs AUTOC to guide optimization of different components of the treatment-planning process has been developed recently by Dolly et. al. [32]. With this framework, one can optimize parameters in pre-treatment imaging such as imaging dose, compare segmentation algorithms and evaluate plan optimization algorithms.

The TOC analysis has to be applied with appropriate caution, because TOC curves constructed from the TCP and the NTCP dose-response curves are subject to moderately large uncertainties. This is because the TCP and the NTCP models are estimated from limited amounts of clinical data focused on the relatively low-dose range. Further discussions on uncertainties in TOC curves and precautions to take when using the curves can be found in Metz et. al. [26] . We examined uncertainties due to varying model parameters in Supplement B, the results show that there are uncertainties in the AUTOC values, but the trend of the AUTOC–vs.–motion plot does not change much. Furthermore, fractionation schedule may introduce uncertainties to the TOC analysis. The TCP/NTCP models may be derived based on different fractionation schedules; uncertainties in converting doses between different fractionation schemes may affect the TOC analysis.

Dose scaling is used in the TOC analysis to generate TCP and NTCP at varying overall dose levels. When compared in terms of AUTOC, the clinical dose-escalated plans are not significantly different from the original plans. Dose scaling is reasonable at least for the purpose of evaluating the effects of motion. Moreover, in emerging research of personalized-dose prescription, there is a renewed interest in changing the overall dose after a treatment plan has been generated [33, 58–61]. If such a treatment regimen is used, a TOC curve, with the overall dose as the hidden variable, provides a full picture of the trade-offs between the risks and the benefits, independent of the dose level.

An important limitation of our work is that we used pancreatic data but did not use a pancreatic SBRT TCP model. SBRT is emerging as an attractive therapeutic option for patients with pancreatic tumors. However, since higher doses per fraction are only beginning to see widespread use, there is a lack of quality clinical data relating dose distributions and outcomes for these high-dose treatments. As a result, there is little consensus to date on TCP models of pancreatic SBRT. TCP models of high-dose treatments to the lung, brain, head and neck, and liver have been published recently [22, 53, 62]. Since these models were based on similar dose fractionation schemes as pancreatic SBRT, they might provide

reasonable estimates for the TCP in pancreatic SBRT. Therefore, TCP models based on lung and liver SBRT data (Supplement A) were considered to approximate local control of pancreatic SBRT. Future clinical trials of pancreatic SBRT will provide better guidance in this regard.

Another limitation is that we assumed rigid motion of the pancreas and the duodenum. The pancreas can undergo deformation up to 5 mm during respiration, yet on average the tumor borders are deformed by only 1—2 mm [41]. The deformation is small compared to the typical magnitude of pancreatic motion (1—2 cm) [5]. One study [63] compared rigid and deformable dose accumulation in liver SBRT and found that the rigid dose accumulation led to dose errors averaging less than 1% of the prescription dose for the tumor and the normal tissue (ranging from −5.1%—8.3%). With these data, we think that rigid motion is a reasonable approximation. However, future work on this topic may include the effects of deformation (perhaps using intrafraction images obtained from MR-equipped linacs).

V. CONCLUSIONS

In conclusion, we presented TOC as a tool and AUTOC as a figure of merit to objectively quantify the effects of motion on treatment efficacy. We demonstrated the application of TOC and AUTOC with clinical data while studying the motion sensitivity of pancreatic SBRT treatment plans. We were able to identify motion-sensitive plans and explore the cause of the motion sensitivity. Furthermore, we explored the uncertainties in the TOC analysis.

ACKNOWLEDGEMENTS

The authors at the University of Colorado were funded in part by the NIH K12-CA086913, the University of Colorado Cancer Center/ACS IRG#57-001-53, the Boettcher Foundation, and Varian Medical Systems. The authors at the University of Arizona were supported by NIH 5-P41-EB002035 and R01-EB000803. The authors would like to thank Dr. Michael A. King for his valuable feedback on the manuscript.

DISCLOSURE OF CONFLICTS OF INTEREST

Drs. Jones and Miften have filed a provisional patent application for the fiducial marker tracking technique used in the collection of tumor motion data. Other authors have no relevant conflicts of interest to disclose.

REFERENCES

[1] Kitamura Kei, Shirato Hiroki, Seppenwoolde Yvette, et al. Three-dimensional intrafractional movement of prostate measured during real-time tumor-tracking radiotherapy in supine and prone treatment positions *International Journal of Radiation Oncology Biology Physics.* 2002;53:1117–1123.

[2] Weiss Elisabeth, Vorwerk Hilke, Richter Susanne, Hess Clemens F. Interfractional and intrafractional accuracy during radiotherapy of gynecologic carcinomas: a comprehensive evaluation using the ExacTrac system *International Journal of Radiation Oncology Biology Physics.* 2003;56:69–79.

[3] George R, Keall PJ, Kini VR, et al. Quantifying the effect of intrafraction motion during breast IMRT planning and dose delivery *Medical Physics.* 2003;30:552–562.

[4] Purdie Thomas G, Bissonnette Jean-Pierre, Franks Kevin, et al. Cone-beam computed tomography for on-line image guidance of lung stereotactic radiotherapy: localization, verification, and intrafraction tumor position *International Journal of Radiation Oncology Biology Physics.* 2007;68:243–252.

[5] Campbell Warren G, Jones Bernard L, Schefter Tracey, Goodman Karyn A, Miften Moyed. An evaluation of motion mitigation techniques for pancreatic SBRT *Radiotherapy and Oncology.* 2017.

[6] Jiang Steve B, Pope Cynthia, Al Jarrah Khaled M, Kung Jong H, Bortfeld Thomas, Chen George TY. An experimental investigation on intra-fractional organ motion effects in lung IMRT treatments *Physics in Medicine & Biology.* 2003;48:1773.

[7] Herk Marcel, Remeijer Peter, Rasch Coen, Lebesque Joos V. The probability of correct target dosage: dose-population histograms for deriving treatment margins in radiotherapy *International Journal of Radiation Oncology Biology Physics.* 2000;47:1121–1135.

[8] Stroom Joep C, Boer Hans CJ, Huizenga Henk, Visser Andries G. Inclusion of geometrical uncertainties in radiotherapy treatment planning by means of coverage probability *International Journal of Radiation Oncology Biology Physics.* 1999;43:905–919.

[9] Barrett Harrison H. Objective assessment of image quality: effects of quantum noise and object variability *JOSA A.* 1990;7:1266–1278.

[10] Chakraborty Dev P, Berbaum Kevin S. Observer studies involving detection and localization: modeling, analysis, and validation *Medical physics.* 2004;31:2313–2330.

[11] Clarkson Eric. Estimation receiver operating characteristic curve and ideal observers for combined detection/estimation tasks *JOSA A.* 2007;24:B91–B98.

[12] Okunieff Paul, Morgan David, Niemierko Andrzej, Suit Herman D. Radiation dose-response of human tumors *International Journal of Radiation Oncology Biology Physics.* 1995;32:1227–1237.

[13] Niemierko Andrzej, Goitein Michael. Implementation of a model for estimating tumor control probability for an inhomogeneously irradiated tumor *Radiotherapy and Oncology.* 1993;29:140–147.

[14] Lyman John T. Complication probability as assessed from dose-volume histograms *Radiation Research.* 1985;104:S13–S19.

[15] Kutcher Gerald J, Burman C. Calculation of complication probability factors for non-uniform normal tissue irradiation: The effective volume method *International Journal of Radiation Oncology Biology Physics.* 1989;16:1623–1630.

[16] Allen Li X, Alber Markus, Deasy Joseph O, et al. The use and QA of biologically related models for treatment planning: Short report of the TG-166 of the therapy physics committee of the AAPM *Medical Physics.* 2012;39:1386–1409.

[17] Sanchez-Nieto B, Nahum AE. BIOPLAN: software for the biological evaluation of radiotherapy treatment plans *Medical Dosimetry.* 2000;25:71–76.

[18] Warkentin Brad, Stavrev Pavel, Stavreva Nadia, Field Colin, Fallone B Gino. A TCP-NTCP estimation module using DVHs and known radiobiological models and parameter sets *Journal of Applied Clinical Medical Physics.* 2004;5:50–63.

[19] Gay Hiram A, Niemierko Andrzej. A free program for calculating EUD-based NTCP and TCP in external beam radiotherapy *Physica Medica.* 2007;23:115–125.

[20] Bentzen Søren M, Constine Louis S, Deasy Joseph O, et al. Quantitative Analyses of Normal Tissue Effects in the Clinic (QUANTEC): an introduction to the scientific issues *International Journal of Radiation Oncology Biology Physics.* 2010;76:S3–S9.

[21] Miften Moyed, Vinogradskiy Yevgeniy, Moiseenko Vitali, et al. Radiation dose-volume effects for liver SBRT *International Journal of Radiation Oncology Biology Physics.* 2018.

[22] Vargo JA, Moiseenko V, Grimm J, et al. Head and Neck Tumor Control Probability: Radiation Dose-Volume Effects in Stereotactic Body Radiation Therapy for Locally Recurrent Previously-Irradiated Head and Neck Cancer: Report of the AAPM Working Group. *International Journal of Radiation Oncology Biology Physics.* 2018.

[23] Moore Dan H, Mendelsohn Mortimer L. Optimal treatment levels in cancer therapy *Cancer.* 1972;30:97–106.

[24] Mendelsohn M. L.. Radiotherapy and Tolerance in *Frontiers of Radiation Therapy and Oncology* (Vaeth Jerome M. , ed.);6:512–523Baltimore, Maryland: University Park Press 1972.

[25] Tokars Roger P, Griem Melvin L. Carcinoma of the nasopharynx an optimization of radiotherapeutic management for tumor control and spinal cord injury *International Journal of Radiation Oncology Biology Physics.* 1979;5:1741–1748.

[26] Metz Charles E, Tokars Roger P, Kronman Helen B, Griem Melvin L. Maximum likelihood estimation of dose-response parameters for therapeutic operating characteristic (TOC) analysis of carcinoma of the nasopharynx *International Journal of Radiation Oncology Biology Physics.* 1982;8:1185–1192.

[27] Ågren Annakarin, Brahme Anders, Turesson Ingela. Optimization of uncomplicated control for head and neck tumors *International Journal of Radiation Oncology Biology Physics.* 1990;19:1077–1085.

[28] Andrews J Robert. Benefit, risk, and optimization by ROC analysis in cancer radiotherapy *International Journal of Radiation Oncology Biology Physics.* 1985;11:1557–1562.

[29] Hanley James A, McNeil Barbara J. The meaning and use of the area under a receiver operating characteristic (ROC) curve. *Radiology.* 1982;143:29–36.

[30] Barrett Harrison H, Kupinski Matthew A, Müeller Stefan, Halpern Howard J, Morris III John C, Dwyer Roisin. Objective assessment of image quality VI: Imaging in radiation therapy

Physics in Medicine & Biology. 2013;58:8197.

[31] Barrett Harrison H, Wilson Donald W, Kupinski Matthew A, et al. Therapy operating characteristic (TOC) curves and their application to the evaluation of segmentation algorithms in *Medical Imaging 2010: Image Perception, Observer Performance, and Technology Assessment*;7627:76270ZInternational Society for Optics and Photonics 2010.

[32] Dolly Steven R, Anastasio Mark A, Yu Lifeng, Li Hua. Task-based image quality assessment in radiation therapy: initial characterization and demonstration with CT simulation images in *Medical Imaging 2017: Image Perception, Observer Performance, and Technology Assessment*;10136:101360YInternational Society for Optics and Photonics 2017.

[33] Hoffmann Aswin L, Huizenga Henk, Kaanders Johannes HAM. Employing the therapeutic operating characteristic (TOC) graph for individualised dose prescription *Radiation Oncology.* 2013;8:55.

[34] Barrett Harrison H, Alberts David S, Woolfenden James M, Caucci Luca, Hoppin John W. Therapy operating characteristic curves: tools for precision chemotherapy *Journal of Medical Imaging.* 2016;3:023502.

[35] Herman Joseph M., Chang Daniel T., Goodman Karyn A., et al. Phase 2 multi-institutional trial evaluating gemcitabine and stereotactic body radiotherapy for patients with locally advanced unresectable pancreatic adenocarcinoma *Cancer.* 2015;121:1128–1137.

[36] Chuong Michael D, Springett Gregory M, Freilich Jessica M, et al. Stereotactic body radiation therapy for locally advanced and borderline resectable pancreatic cancer is effective and well tolerated *International Journal of Radiation Oncology Biology Physics.* 2013;86:516–522.

[37] Chang Daniel T, Schellenberg Devin, Shen John, et al. Stereotactic radiotherapy for unresectable adenocarcinoma of the pancreas *Cancer.* 2009;115:665–672.

[38] Koong Albert C, Christofferson Erin, Le Quynh-Thu, et al. Phase II study to assess the efficacy of conventionally fractionated radiotherapy followed by a stereotactic radiosurgery boost in patients with locally advanced pancreatic cancer *International Journal of Radiation Oncology Biology Physics.* 2005;63:320–323.

[39] Jones Bernard L, Schefter Tracey, Miften Moyed. Adaptive motion mapping in pancreatic SBRT patients using Fourier transforms *Radiotherapy and Oncology.* 2015;115:217–222.

[40] Ge Jiajia, Santanam Lakshmi, Noel Camille, Parikh Parag J. Planning 4-dimensional computed tomography (4DCT) cannot adequately represent daily intrafractional motion of abdom-

inal tumors *International Journal of Radiation Oncology Biology Physics.* 2013;85:999–1005.

[41] Feng Mary, Balter James M, Normolle Daniel, et al. Characterization of pancreatic tumor motion using cine MRI: surrogates for tumor position should be used with caution *International Journal of Radiation Oncology Biology Physics.* 2009;74:884–891.

[42] Hoyer Morten, Roed Henrik, Sengelov Lisa, et al. Phase-II study on stereotactic radiotherapy of locally advanced pancreatic carcinoma *Radiotherapy and Oncology.* 2005;76:48–53.

[43] Bortfeld Thomas, Jokivarsi Kimmo, Goitein Michael, Kung Jong, Jiang Steve B. Effects of intra-fraction motion on IMRT dose delivery: statistical analysis and simulation *Physics in Medicine & Biology.* 2002;47:2203.

[44] Bengt K. Lind Simo Hyödynmaa, Kappas Constantin. Optimization of the dose level for a given treatment plan to maximize the complication-free tumor cure *Acta Oncologica.* 1999;38:787–798.

[45] Munro TR, Gilbert CW. The relation between tumour lethal doses and the radiosensitivity of tumour cells *The British journal of radiology.* 1961;34:246–251.

[46] Brenner David J. The linear-quadratic model is an appropriate methodology for determining isoeffective doses at large doses per fraction in *Seminars in radiation oncology*;18:234–239Elsevier 2008.

[47] Withers H Rodney, Taylor Jeremy MG, Maciejewski Boguslaw. Treatment volume and tissue tolerance *International Journal of Radiation Oncology Biology Physics.* 1988;14:751–759.

[48] Fowler Jack F. 21 years of biologically effective dose *The British journal of radiology.* 2010;83:554–568.

[49] Murphy James D, Christman-Skieller Claudia, Kim Jeff, Dieterich Sonja, Chang Daniel T, Koong Albert C. A dosimetric model of duodenal toxicity after stereotactic body radiotherapy for pancreatic cancer *International Journal of Radiation Oncology Biology Physics.* 2010;78:1420–1426.

[50] Campbell Warren G, Miften Moyed, Jones Bernard L. Automated target tracking in kilovoltage images using dynamic templates of fiducial marker clusters *Medical Physics.* 2017;44:364–374.

[51] Jones Bernard L, Westerly David, Miften Moyed. Calculating tumor trajectory and dose-of-the-day using cone-beam CT projections *Medical Physics.* 2015;42:694–702.

[52] Poulsen Per Rugaard, Cho Byungchul, Keall Paul J. A method to estimate mean position, motion magnitude, motion correlation, and trajectory of a tumor from cone-beam CT projections for image-guided radiotherapy *International Journal of Radiation Oncology Biology Physics.* 2008;72:1587–1596.

[53] Shuryak Igor, Carlson David J, Brown J Martin, Brenner David J. High-dose and fractionation effects in stereotactic radiation therapy: Analysis of tumor control data from 2965 patients *Radiotherapy and Oncology.* 2015;115:327–334.

[54] US Department of Health and Human Services , others . Common terminology criteria for adverse events (CTCAE) version 3.0 *National Cancer Institute.* 2006.

[55] Shirato Hiroki, Seppenwoolde Yvette, Kitamura Kei, Onimura Rikiya, Shimizu Shinichi. Intrafractional tumor motion: lung and liver in *Seminars in radiation oncology*;14:10–18Elsevier 2004.

[56] Seppenwoolde Yvette, Shirato Hiroki, Kitamura Kei, et al. Precise and real-time measurement of 3D tumor motion in lung due to breathing and heartbeat, measured during radiotherapy *International Journal of Radiation Oncology Biology Physics.* 2002;53:822–834.

[57] Chu Millie, Zinchenko Yuriy, Henderson Shane G, Sharpe Michael B. Robust optimization for intensity modulated radiation therapy treatment planning under uncertainty *Physics in Medicine & Biology.* 2005;50:5463.

[58] Baardwijk Angela, Bosmans Geert, Bentzen Søren M, et al. Radiation Dose Prescription for Non–Small-Cell Lung Cancer According to Normal Tissue Dose Constraints: An In Silico Clinical Trial *International Journal of Radiation Oncology Biology Physics.* 2008;71:1103–1110.

[59] Hoffmann Aswin L, Troost Esther GC, Huizenga Henk, Kaanders Johannes HAM, Bussink Johan. Individualized dose prescription for hypofractionation in advanced non-small-cell lung cancer radiotherapy: an in silico trial *International Journal of Radiation Oncology Biology Physics.* 2012;83:1596–1602.

[60] Uzan J, Nahum AE. Radiobiologically guided optimisation of the prescription dose and fractionation scheme in radiotherapy using BioSuite *The British journal of radiology.* 2012;85:1279–1286.

[61] Vinogradskiy Yevgeniy, Tucker Susan L, Bluett Jaques B, Wages Cody A, Liao Zhongxing, Martel Mary K. Prescribing radiation dose to lung cancer patients based on personalized

toxicity estimates *Journal of Thoracic Oncology.* 2012;7:1676–1682.

[62] Ohri Nitin, Tomé Wolfgang A, Romero Alejandra Méndez, et al. Local Control following Stereotactic Body Radiation Therapy for Liver Tumors *International Journal of Radiation Oncology Biology Physics.* 2018.

[63] Velec Michael, Moseley Joanne L, Eccles Cynthia L, et al. Effect of breathing motion on radiotherapy dose accumulation in the abdomen using deformable registration *International Journal of Radiation Oncology Biology Physics.* 2011;80:265–272.